Fizika Nizkikh Temperatur, 2004, v. 30, No. 4, p. 411–426

Electronic structure and x-ray magnetic circular dichroism in uranium monochalcogenides

V.N. Antonov* and B.N. Harmon

Ames Laboratory, Iowa State University, Iowa 50011, USA
E-mail: antonov@ameslab.gov; antonov@imp.kiev.ua

O.V. Andryushchenko and L.V. Bekenev

Institute of Metal Physics, 36 Vernadsky Str., Kiev 03142, Ukraine

A.N. Yaresko

Max Planck Institute for Physics of Complex Systems, Dresden D-01187, Germany

Received August 7, 2003, revised October 21, 2003

The electronic structure and x-ray magnetic circular dichroism (XMCD) spectra of US, USe, and UTe are investigated theoretically from first principles, using the fully relativistic Dirac LMTO band structure method. The electronic structure is obtained with the local spin-density approximation (LSDA), as well as with a generalization of the LSDA+*U* method which takes into account that in the presence of spin–orbit coupling the occupation matrix of localized electrons becomes non-diagonal in spin indexes. The origin of the XMCD spectra in the compounds is examined.

PACS: 7**1.28.+d**, 71.25.Pi, 75.30.Mb

1. Introduction

The uranium compounds US, USe, and UTe belong to the class of uranium monochalcogenides that crystallize in the NaCl structure and order ferromagnetically (on the uranium sublattice) at Curie temperatures of 178, 160, and 102 K, respectively (see, e.g., the review [1]). These uranium compounds exhibit several unusual physical phenomena, which are the reason for a continuing ongoing interest in these compounds. Despite their relatively simple and highly symmetrical NaCl structure, it has been found that the magnetic ordering on the uranium atoms is strongly anisotropic [2,3], with the uranium moment favoring a [111] alignment. The magnetic anisotropy in US, e.g., is one of the largest measured in a cubic material, with a magnetic anisotropy constant K_1 of more than $2 \cdot 10^8$ erg/cm^3 [4]. Also the magnetic moment itself is unusual, consisting of an orbital moment that is about twice as large as the spin moment, and of opposite sign [5–7]. A bulk magnetization measurement [3] yields an ordered moment of 1.55 μ_B per unit formula, and neutron scattering measurements [8] show a slightly larger value of 1.70 μ_B, which is assigned to the 5*f* magnetic moment. These values are far smaller than that expected for the free ion, indicating that some sort of «solid state effect» takes place with the 5*f* states. From several experimental results (for instance, photoemission [9], electrical resistivity [10], pressure dependence of Curie temperature [11], and specific heat measurements [12,13],) the 5*f* electrons of US are considered to be itinerant.

It has been suggested that uranium monochalcogenides are mixed valence systems [14]. Low-temperature ultrasonic studies on USe and UTe were performed in the context of questioning the possibility of the coexistence of magnetism and intermediate valence behavior [15]. They found a monotonic trend of the Poisson's ratio, which decreases with increasing chalcogenide mass and is positive in US, negative in USe, and UTe. This indicates the possibility of intermediate valence in the last two compounds. Indeed, a

* Permanent address: Institute of Metal Physics, 36 Vernadsky Str., Kiev 03142, Ukraine

negative Poisson's ratio, i.e. a negative C_{12} elastic constant, is quite common for intermediate valence systems, and its occurrence seems to be due to an anomalously low value of the bulk modulus. A negative C_{12} means that it costs more energy to distort the crystal from cubic to tetragonal structure than to modify the volume. Thus, when uniaxially compressed along a [100] direction, the material will contract in the [010] and [001] directions, trying to maintain a cubic structure. An explanation for a negative C_{12} may be given through a breathing deformability of the actinide ion due to a valence instability [16].

The dependence of the Curie temperatures T_C of US, USe and UTe on hydrostatic pressure up to 13 GPa has been determined in Ref. 17. For USe and UTe, T_C initially increases with applied pressures, passing through maxima at pressure of about 6 GPa and 7 GPa, respectively. For US, T_C decreases monotonically with pressure, which is consistent with pressure-dependent itinerant electron magnetism. Pressure increases the bandwidth and correspondingly decreases the density of states at the Fermi level, which leads to a decrease of T_C. The behavior of USe and UTe is suggestive of localized interacting $5f$ moments undergoing Kondo-type fluctuations, which begin to exceed the magnetic interaction when T_C passes through a maximum. A theoretical analysis of these experiments is given in Ref. 18. On the basis of band structure calculations it is argued that the nonmonotonic behavior of T_C under pressure is solely the result of pressure-driven increased $5f$ itineracy.

It must be remarked that the behavior of uranium monochalcogenides cannot be explained entirely by a simple trend of increasing localization with increasing chalcogen mass [19]. Whereas such a trend is evident in the dynamic magnetic response, in the pressure dependence of the Curie temperatures and in the value of the ordered moment, the behavior of Poisson's ratio and of the Curie temperature is the opposite from what one would naively expect.

There are several band structure calculations of uranium monochalcogenides in the literature [7, 20–28]. Kraft et al. [23] have performed the local spin–density approximation (LSDA) calculation with the spin–orbit interaction (SOI) in a second variational treatment for ferromagnetic uranium monochalcogenides (US, USe, and UTe) using the ASW method, and have shown that the magnitude of the calculated orbital magnetic moment M_l is larger than that of spin moment M_s and they couple to each other in an antiparallel way. However, the magnitude of the total magnetic moment ($M_s + M_l$) is too small compared to the experimental data, indicating that the calculated M_l is not large enough.

The optical and magnetooptical (MO) spectra of uranium monochalcogenides have been investigated theoretically in Refs. 20,21,23,25. These theoretical spectra are all computed from first principles, using Kubo linear-response theory, but it appears that there are large differences among them. Cooper and coworkers [22] find good agreement with experiment for the real part of the diagonal conductivity ($\sigma^{(1)}_{xx}$) of UTe, but the much more complicated off-diagonal conductivity ($\sigma^{(2)}_{xy}$) of US and UTe is about 4 times larger than experiment, and also the shape of their spectrum is different from the experimental one. Halilov and Kulatov [20] also find an off-diagonal conductivity which is much larger than the experimental one, but they additionally obtain a diagonal conductivity $\sigma^{(1)}_{xx}$ that differs substantially from experiment. Gasche [21] find a Kerr rotation spectrum of US that is quite different from experiment, and subsequently consider the effect of an orbital polarization term to improve the ab initio Kerr spectra. Kraft et al. [23] obtained for US, USe, and UTe reasonable agreement with experiment for the absolute value of the Kerr spectra. However, the shape of the Kerr spectra is not reproduced by LSDA theory, since the theoretical spectra exhibit a double-peak structure but the experimental spectra have only a one-peak structure. The LSDA+U calculations presented in Ref. 25 take into account the strong Coulomb correlations among the $5f$ orbitals and are greatly improve the agreement between theory and experiment for all three materials. This finding appears to be consistent with the quasilocalized nature of the $5f$ electrons in these compounds.

X-ray magnetic circular dichroism (XMCD) technique has developed in recent years into a powerful magnetometry tool to investigate orbital and spin contributions to magnetic moments. XMCD measures the difference in absorption of a compound for x rays with the two opposite (left and right) states of circular polarization. The study of the $5f$ electron shell in uranium compounds is usually performed by tuning the energy of the x-ray close to the $M_{4,5}$ edges of uranium (located at 3552 and 3728 eV, respectively) where electronic transitions between $3d_{3/2,5/2}$ and $5f_{5/2,7/2}$ states are involved. Recently XMCD measurements have been successfully performed on US at the $M_{4,5}$ edges [29]. The XMCD spectrum for U $3d \to 5f$ transitions in US has been calculated in Ref. 27 on the basis of the HF approximation for an extended Hubbard model. The parameters involved in the tight-binding model were determined by fitting the energy of Bloch electrons in the paramagnetic state obtained in LDA band structure calculation.

There are no XMCD calculations for USe and UTe in the literature.

With the aim of undertaking a systematic investigation of the trends in uranium compounds we present the theoretically calculated electronic structure and XMCD spectra at $M_{4,5}$ edges for the UX (X — S, Se, and Te) compounds.

The paper is organized as follows. Section 2 presents a description of the crystal structure of the U monochalcogenides and the computational details. Section 3 is devoted to the electronic structure and XMCD spectra of US, USe, and UTe calculated in the LSDA and LSDA+U approximations. The XMCD theoretical calculations are compared to the experimental measurements. Finally, the results are summarized in Sec. 4.

2. Computational details

Magnetooptical effects refer to various changes in the polarization state of light upon interaction with materials possessing a net magnetic moment, including rotation of the plane of linearly polarized light (Faraday, Kerr rotation), and the complementary differential absorption of left and right circularly polarized light (circular dichroism). In the near-visible spectral range these effects result from excitation of electrons in the conduction band. Near x-ray absorption edges, or resonances, magnetooptical effects can be enhanced by transitions from well-defined atomic core levels to transition symmetry selected valence states. There are at least two alternative formalisms for describing resonant soft x-ray MO properties. One uses the classical dielectric tensor [30]. Another uses the resonant atomic scattering factor including charge and magnetic contributions [31,32]. The equivalence of these two descriptions (within the dipole approximation) is demonstrated in Ref. 33.

For the polar Kerr magnetization geometry and a crystal of tetragonal symmetry, where both the fourfold axis and the magnetization **M** are perpendicular to the sample surface and the z axis is chosen parallel to them, the dielectric tensor is composed of the diagonal ε_{xx} and ε_{zz} components and the off-diagonal ε_{xy} component in the form

$$\varepsilon = \begin{pmatrix} \varepsilon_{xx} & \varepsilon_{xy} & 0 \\ -\varepsilon_{xy} & \varepsilon_{xx} & 0 \\ 0 & 0 & \varepsilon_{zz} \end{pmatrix}. \qquad (1)$$

A complete description of MO effects in this formalism is given by the four nonzero elements of the dielectric tensor or, equivalently, by the complex refractive index $n(\omega)$

$$n(\omega) \equiv \sqrt{\varepsilon(\omega)} = 1 - \delta(\omega) + i\beta(\omega) \qquad (2)$$

for several normal modes corresponding to the propagation of pure polarization states along specific directions in the sample. The solution of Maxwell's equations yields these normal modes [34]. One of these modes is for circular components of opposite (±) helicity with wave vector $\mathbf{h}||\mathbf{M}$ having indexes

$$n_{\pm} = 1 - \delta_{\pm} + i\beta_{\pm} = \sqrt{\varepsilon_{xx} \pm i\varepsilon_{xy}}. \qquad (3)$$

The two other cases are for linear polarization with $\mathbf{h}\perp\mathbf{M}$ [33]. One has electric vector $\mathbf{E}||\mathbf{M}$ and index $n_{||} = 1 - \delta_{||} + i\beta_{||} = \sqrt{\varepsilon_{zz}}$. The other has $\mathbf{E}\perp\mathbf{M}$ and $n_{\perp} = 1 - \delta_{\perp} + i\beta_{\perp} = \sqrt{(\varepsilon_{xx}^2 + \varepsilon_{xy}^2) \,/\, \varepsilon_{xx}}$.

At normal light incidence the complex Faraday angle is given by [33,35]

$$\varphi_F(\omega) = \theta_F(\omega) - i\eta_F(\omega) = \frac{\omega l}{2c}(n_+ - n_-). \qquad (4)$$

where c is the speed of light, and $\theta_F(\omega)$ and $\eta_F(\omega)$ are the Faraday rotation and the ellipticity. The complex Faraday response describes the polarization changes to the incident linear polarization on propagation through the film of thickness l. (The incident linearly polarized light is a coherent superposition of two circularly waves of opposite helicity.)

Magnetic circular dichroism is of first order in M (or ε_{xy}) and is given by $\beta_+ - \beta_-$ or $\delta_+ - \delta_-$, respectively, the later representing the magnetooptical rotation (MOR) of the plane of polarization (Faraday effect). Magnetic linear dichroism (MLD) $n_{\perp} - n_{||}$ (also known as the Voigt effect) is quadratic in M. The Voigt effect is present in both ferromagnets and antiferromagnets, while the first-order MO effects in the forward scattering beam are absent with the net magnetization in antiferromagnets.

The alternative consideration of the MO effects is based on the atomic scattering factor $f(\omega,q)$, which provides a microscopic description of the interaction of x-ray photons with magnetic ions. For forward scattering $(q = 0)$ $f(\omega) = Z + f'(\omega) + if''(\omega)$, where Z is the atomic number. $f'(\omega)$ and $f''(\omega)$ are the anomalous dispersion corrections related to each other by the Kramers–Kronig transformation. The general equivalence of these two formalisms can be seen by noting the one-to-one correspondence of terms describing the same polarization dependence for the same normal modes [33]. For a multicomponent sample they relate to δ and β through:

$$\delta(\omega) = \frac{2\pi c^2 r_e}{\omega^2} \sum_i Z_i f_i'(\omega) N_i, \qquad (5)$$

$$\beta(\omega) = \frac{2\pi c^2 r_e}{\omega^2} \sum_i f_i''(\omega) N_i , \qquad (6)$$

where the sum is over atomic spheres, each having number density N_i, and r_e is the classical electron radius. The x-ray absorption coefficient $\mu^\lambda(\omega)$ of polarization λ may be written in terms of the imaginary part of $f_\lambda(\omega)$ as

$$\mu^\lambda(\omega) = \frac{4\pi r_e c}{\Omega\omega} f_\lambda''(\omega), \qquad (7)$$

where Ω is the atomic volume. The x-ray MCD, which is the difference in x-ray absorption for right- and left-circularly polarized photons ($\mu^+ - \mu^-$) can be represented by ($f_+'' - f_-''$). Faraday rotation $\theta_F(\omega)$ of linear polarization measures the MCD in the real part f_λ' of the resonant magnetic x-ray-scattering amplitude, i.e [36]

$$\theta_F(\omega) = \frac{\omega l}{2c} \mathrm{Re}\,[n_+ - n_-] = \frac{\pi l r_e}{\Omega\omega} (f_-'(\omega) - f_+'(\omega)) . \qquad (8)$$

Finally, the x-ray scattering intensity from an elemental magnet at the Bragg reflection measured in the resonant magnetic x-ray-scattering experiments is just the squared modulus of the total scattering amplitude, which is a linear combination of $(f_\pm' + if_\pm'', f_z'' + if_z'')$ with the coefficients fully determined by the experimental geometry [35]. Multiple scattering theory is usually used to calculate the resonant magnetic x-ray scattering amplitude $(f' + if'')$ [30,35,37].

We should mention that the general equivalence of the dielectric tensor and scattering factor descriptions holds only in the case considering dipole transitions contributing to the atomic scattering factor $f(\omega)$. Higher-order multipole terms have different polarization dependence [31].

Using straightforward symmetry considerations it can be shown that all magnetooptical phenomena (XMCD, MO Kerr and Faraday effects) are caused by symmetry reduction, in comparison to the paramagnetic state, caused by magnetic ordering [38]. XMCD properties are manifested only when SO coupling is considered in addition. To calculate the XMCD properties one has to account for magnetism and SO coupling at the same time when dealing with the electronic structure of the material considered. The theoretical description of magnetic dichroism can be cast into four categories. On the one hand, there are one-particle (ground-state) and many-body (excited-state) theories; on the other hand, there are theories for single atoms and those which take into account the solid state. To name a few from each category, for atomic one-particle theories we refer to Refs. 39 and 40, for atomic many-particle multiplet theory to Refs. 41–44, for solid many-particle theories to Ref. 45, and for solid one-particle theories (photoelectron diffraction) to Refs. 46–49. A multiple-scattering approach to XMCD, a solid-state one-particle theory, has been proposed by Ebert et al. [50–52] and Tamura et al. [53].

Within the one-particle approximation, the absorption coefficient μ for an incident x ray of polarization λ and photon energy $\hbar\omega$ can be determined as the probability of electron transition from an initial core state (with wave function ψ_j and energy E_j) to a final unoccupied state (with wave function $\psi_{n\mathbf{k}}$ and energy $E_{n\mathbf{k}}$)

$$\mu_j^\lambda(\omega) = \sum_{n\mathbf{k}} |\langle \Psi_{n\mathbf{k}} | \Pi_\lambda | \Psi_j \rangle|^2 \times$$
$$\times \delta (E_{n\mathbf{k}} - E_j - \hbar\omega)\, \theta (E_{n\mathbf{k}} - E_F) . \qquad (9)$$

The Π_λ is the dipole electron–photon interaction operator

$$\Pi_\lambda = - e\alpha \mathbf{a}_\lambda , \qquad (10)$$

where α are the Dirac matrices, and $\mathbf{a}_\lambda$ is the λ polarization unit vector of the photon potential vector [$a_\pm = 1/\sqrt{2}(1, \pm i, 0)$, $a_z = (0, 0, 1)$]. (Here $+/-$ denotes, respectively, left and right circular photon polarizations with respect to the magnetization direction in the solid.) More detailed expressions of the matrix elements for the spin-polarized fully relativistic LMTO method may be found in Refs. 52,54.

While XMCD is calculated using equation (9), the main features can be understood already from a simplified expression for paramagnetic solids. With restriction to electric dipole transitions, keeping the integration only inside the atomic spheres (due to the highly localized core sates) and averaging with respect to polarization of the right, one obtains the following expression for the absorption coefficient of the core level with (l, j) quantum numbers [55]:

$$\mu_{lj}^0(\omega) = \sum_{l', j'} \frac{2j+1}{4} \left(\frac{\delta_{l', l+1} \delta_{j', j+1}}{j+1} + \frac{\delta_{l', l-1} \delta_{j', j-1}}{j} + \right.$$
$$\left. + \frac{\delta_{l', l+1} \delta_{j', j}}{j(j+1)(2j+1)} \right) N_{l', j'}(E) C_{l,j}^{l', j'}(E) . \qquad (11)$$

where $N_{l', j'}(E)$ is the partial density of empty states and the $C_{l,j}^{l', j'}(E)$ radial matrix elements [55].

Equation (11) allows only transitions with $\Delta l = \pm 1$, $\Delta j = 0, \pm 1$ (dipole selection rules) which means that the absorption coefficient can be interpreted as a direct measure for the sum of (l, j)-resolved DOS curves weighted by the square of the corresponding radial matrix element (which usually is a smooth function of energy). This simple interpretation is also valid for the spin-polarized case [30].

The application of standard LSDA methods to f-shell systems meets with problems in most cases, because of the correlated nature of the f electrons. To account better for the on-site f-electron correlations, we have adopted as a suitable model Hamiltonian that of the LSDA+U approach [56]. The main idea is the same as in the Anderson impurity model [57]: the separate treatment of localized f electrons for which the Coulomb f–f interaction is taken into account by a Hubbard-type term in the Hamiltonian $\frac{1}{2}U\sum_{i\neq j} n_i n_j$ (n_i are the f-orbital occupancies), and delocalized s, p, d electrons for which the local density approximation for the Coulomb interaction is regarded as sufficient.

Hubbard [58,59] was one of the first to point out the importance, in the solid state, of Coulomb correlations which occur inside atoms. The many-body crystal wave function has to reduce to many-body atomic wave functions as the lattice spacing is increased. This limiting behavior is missed in the LDA/DFT. The spectrum of excitations for the shell of an f-electron system is a set of many-body levels describing processes of removing and adding electrons. In the simplified case, when every f electron has roughly the same kinetic energy ε_f and Coulomb repulsion energy U, the total energy of the shell with n electrons is given by $E_n = \varepsilon_{fn} + Un(n-1)/2$ and the excitation spectrum is given by $\varepsilon_n = E_{n+1} - E_n = \varepsilon_f + Un$.

Let us consider an f ion as an open system with a fluctuating number of f electrons. The correct formula for the Coulomb energy of f–f interactions as a function of the number of f electrons N given by the LDA should be $E = UN(N-1)/2$ [60]. If we subtract this expression from the LDA total energy functional and add a Hubbard-like term (neglecting for now exchange and non-sphericity) we will have the following functional:

$$E = E^{LDA} - UN(N-1)/2 + \frac{1}{2}U\sum_{i\neq j} n_i n_j \ . \quad (12)$$

The orbital energies ε_i are derivatives of (12):

$$\varepsilon_i = \frac{\partial E}{\partial n_i} = \varepsilon^{LDA} + U(\frac{1}{2} - n_i). \quad (13)$$

This simple formula gives the shift of the LDA orbital energy $-U/2$ for occupied orbitals ($n_i = 1$) and $+U/2$ for unoccupied orbitals ($n_i = 0$). A similar formula is found for the orbital dependent potential $V_i(\mathbf{r}) = \delta E/\delta n_i(\mathbf{r})$, where the variation is taken not on the total charge density $\rho(\mathbf{r})$ but on the charge density of a particular ith orbital $n_i(\mathbf{r})$:

$$V_i(\mathbf{r}) = V^{LDA}(\mathbf{r}) + U(\frac{1}{2} - n_i). \quad (14)$$

Expression (14) restores the discontinuous behavior of the one-electron potential of the exact density-functional theory.

The functional (12) neglects exchange and non-sphericity of the Coulomb interaction. In the most general rotationally invariant form the LDA + U functional is defined as [61,62]

$$E^{LDA+U}[\rho(\mathbf{r}), \hat{n}] = E^{L(S)DA}[\rho(\mathbf{r})] + E^U(\hat{n}) - E^{dc}(\hat{n}), \quad (15)$$

where $E^{L(S)DA}[\rho(\mathbf{r})]$ is the LSDA (or LDA as in Ref. 60) functional of the total electron spin densities, $E^U(\hat{n})$ is the electron–electron interaction energy of the localized electrons, and $E^{dc}(\hat{n})$ is the so-called «double counting» term which cancels approximately the part of an electron–electron energy which is already included in E^{LDA}. The last two terms are functions of the occupation matrix $\hat{n}$ defined using the local orbitals $\{\varphi_{lm\sigma}\}$.

The matrix $\hat{n} = ||n_{\sigma m,\sigma' m'}||$ generally consists of both spin-diagonal and spin-non-diagonal terms. The latter can appear due to the spin–orbit interaction or a noncollinear magnetic order. Then, the second term in Eq. (15) can be written as [61–63]:

$$E^U = \frac{1}{2}\sum_{\sigma,\sigma',\{m\}} (n_{\sigma m_1,\sigma m_2} U_{m_1 m_2 m_3 m_4} n_{\sigma' m_3,\sigma' m_4} - n_{\sigma m_1,\sigma' m_2} U_{m_1 m_4 m_3 m_2} n_{\sigma' m_3,\sigma m_4}), \quad (16)$$

where $U_{m_1 m_2 m_3 m_4}$ are the matrix elements of the on-site Coulomb interaction which are given by

$$U_{m_1 m_2 m_3 m_4} = \sum_{k=0}^{2l} a^k_{m_1 m_2 m_3 m_4} F^k \ , \quad (17)$$

with F^k being screened Slater integrals for a given l and

$$a^k_{m_1 m_2 m_3 m_4} = \frac{4\pi}{2k+1}\sum_{q=-k}^{k} \langle lm_1|Y_{kq}|lm_2\rangle\langle lm_3|Y^*_{kq}|lm_4\rangle \ . \quad (18)$$

The $\langle lm_1|Y_{kq}|lm_2\rangle$ angular integrals of a product of three spherical harmonics Y_{lm} can be expressed in terms of Clebsch–Gordan coefficients, and Eq. (18) becomes

$$a^k_{m_1 m_2 m_3 m_4} = \delta_{m_1 - m_2 + m_3, m_4} (C^{l0}_{k0,l0})^2 \times C^{lm_1}_{km_1 - m_2, lm_2} C^{lm_4}_{km_1 - m_2, lm_3} . \quad (19)$$

The matrix elements $U_{mmm'm'}$ and $U_{mm'm'm}$ which enter those terms in the sum in Eq. (16) which contain a product of the diagonal elements of the occupation matrix can be identified as pair Coulomb and exchange integrals:

$$U_{mmm'm'} = U_{mm'}, \; U_{mm'm'm} = J_{mm'}. \qquad (20)$$

The averaging of the matrices $U_{mm'}$ and $U_{mm'} - J_{mm'}$ over all possible pairs of m, m' defines the averaged Coulomb U and exchange J integrals which enter the expression for E^{dc}. Using the properties of the Clebsch–Gordan coefficients, one can show that

$$U = \frac{1}{(2l+1)^2} \sum_{mm'} U_{mm'} = F^0, \qquad (21)$$

$$U - J = \frac{1}{2l(2l+1)} \sum_{mm'}{}' (U_{mm'} - J_{mm'}) =$$

$$= F^0 - \frac{1}{2l} \sum_{k=2}^{2l} \left(C^{l0}_{n0,l0} \right)^2 F^k, \qquad (22)$$

where the primed sum is over $m' \neq m$. Equations (21) and (22) allow us to establish the following relation between the average exchange integral J and Slater integrals:

$$J = \frac{1}{2l} \sum_{k=2}^{2l} (C^{l0}_{n0,l0})^2 F^k \;, \qquad (23)$$

or explicitly

$$J = \frac{1}{14}(F^2 + F^4), \text{ for } l = 2, \qquad (24)$$

$$J = \frac{1}{6435}(286F^2 + 195F^4 + 250F^6) \text{ for } l = 3. \qquad (25)$$

The meaning of U has been carefully discussed by Herring [64]. For example, in an f-electron system with n f electrons per atom, U is defined as the energy cost for the reaction

$$2(f^n) \rightarrow f^{n+1} + f^{n-1}, \qquad (26)$$

i.e., the energy cost for moving an f electron between two atoms which both initially had n f electrons. It should be emphasized that U is a renormalized quantity which contains the effects of screening by fast s and p electrons. The number of these delocalized electrons on an atom with $n+1$ f electrons decreases whereas their number on an atom with $n-1$ f electrons increases. The screening reduces the energy cost for the reaction given by Eq. (26). It is worth noting that because of the screening the value of U in L(S)DA + U calculations is significantly smaller then the bare U used in the Hubbard model [58,59].

In principle, the screened Coulomb U and exchange J integrals can be determined from supercell LSDA calculations using Slater's transition state technique [65] or from constrained LSDA calculations [66–68]. Then, the LDA+U method becomes parameter-free. However, in some cases, as for instance for bcc iron [65], the value of U obtained from such calculations appears to be overestimated. Alternatively, the value of U estimated from the photoemission spectroscopy (PES) and x-ray bremsstrahlung isochromat spectroscopy (BIS) experiments can be used. Because of the difficulties with unambiguous determination of U it can be considered as a parameter of the model. Then its value can be adjusted so as to achieve the best agreement of the results of LDA+U calculations with PES or optical spectra. While the use of an adjustable parameter is generally considered an anathema among first-principles practitioners, the LDA+U approach does offer a plausible and practical method for the approximate treatment of strongly correlated orbitals in solids. It has been fond that many properties evaluated with the LDA+U method are not sensitive to small variations of the value of U around some optimal value. Indeed, the optimal value of U determined empirically is often very close to the value obtained from supercell or constrained density functional calculations.

All three chalcogenides, namely, US, USe, and UTe, considered in the present work crystallize in the NaCl type structure (B1) with space group symmetry $Fm3m$. The uranium atom is positioned at (0,0,0) and the chalcogen at (1/2, 1/2, 1/2).

The details of the computational method are described in our previous papers [69,70], and here we only mention several aspects. The calculations were performed using the fully relativistic LMTO method for the experimentally observed lattice constants a = = 5.86, 6.06, and 6.436 Å for US, USe, and UTe, respectively. To improve the potential we include additional empty spheres in the (1/4, 1/4, 1/4) positions. We used the von Barth–Hedin parametrization [71] for the exchange-correlation potential. Brillouin zone (BZ) integrations were performed using the improved tetrahedron method [72] and the charge was obtained self-consistently with 1330 irreducible **k** points. The basis consisted of U s, p, d, f and g; chalcogen s, p and d; empty spheres s and p LMTOs.

We have adopted the LSDA+U method [56] as a different level of approximation to treat the electron–electron correlation. We used a generalization of the LSDA+U method which takes into account that in the presence of spin–orbit coupling the occupation

matrix of localized electrons becomes nondiagonal in spin indexes [61]. Screened Coulomb U and exchange J integrals enter the LSDA+U energy functional as external parameters and have been set to U = 2 eV derived from XPS measurements and J = 0.5 eV.

3. Results and discussion

3.1. Band structure and magnetic moments

In our band structure calculations we have performed two independent fully relativistic spin-polarized calculations. We consider the 5f electrons as: itinerant electrons using the local spin-density approximation; and partly localized using the LSDA+U approximation.

Figure 1 shows the energy band structure of US for both the approximations. The LSDA energy band structure of US can be subdivided into three regions separated by energy gaps. The bands in the lowest region around −15 eV have mostly S s character with a small amount of U sp character mixed in. The next six energy bands are S p bands separated from the s bands by an energy gap of about 6 eV. The width of the S p band is about 4 eV. U 6d bands are broad and extend between −2.5 and 10 eV. The sharp peaks in the DOS just below and above the Fermi energy are due to the $5f_{5/2}$ and $5f_{7/2}$ states, respectively. Figure 1 also shows the energy bands and total density of states of US in the LSDA+U approximation [61,62]. The Coulomb repulsion splits partially occupied U $5f_{5/2}$ states and the LSDA+U calculations give a solution

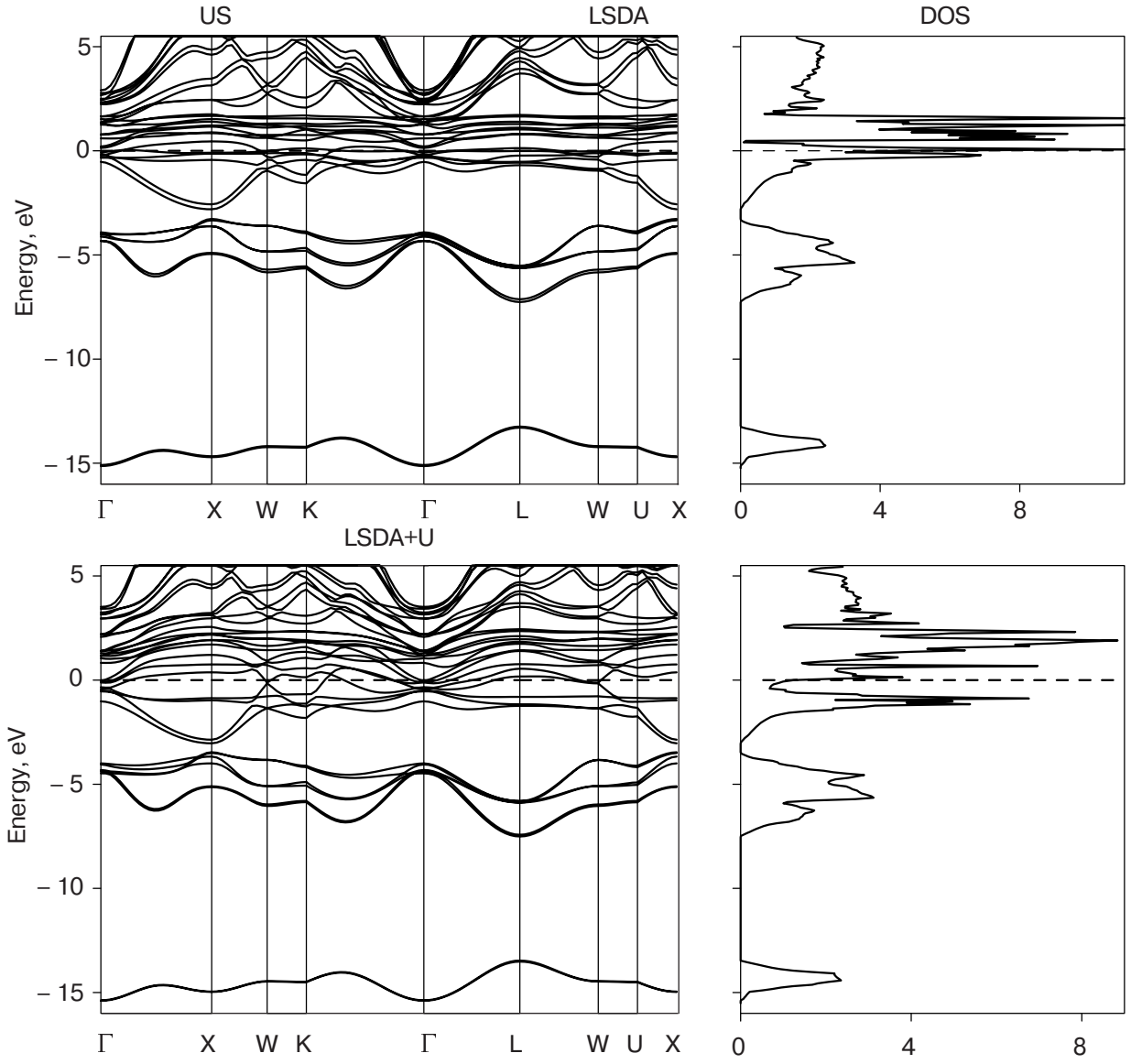

Fig. 1. Self-consistent fully relativistic energy band structure and total DOS (in states/(unit cell·eV)) of US calculated within the LSDA and LSDA+U approximations with U = 2 eV and J = 0.5 eV.

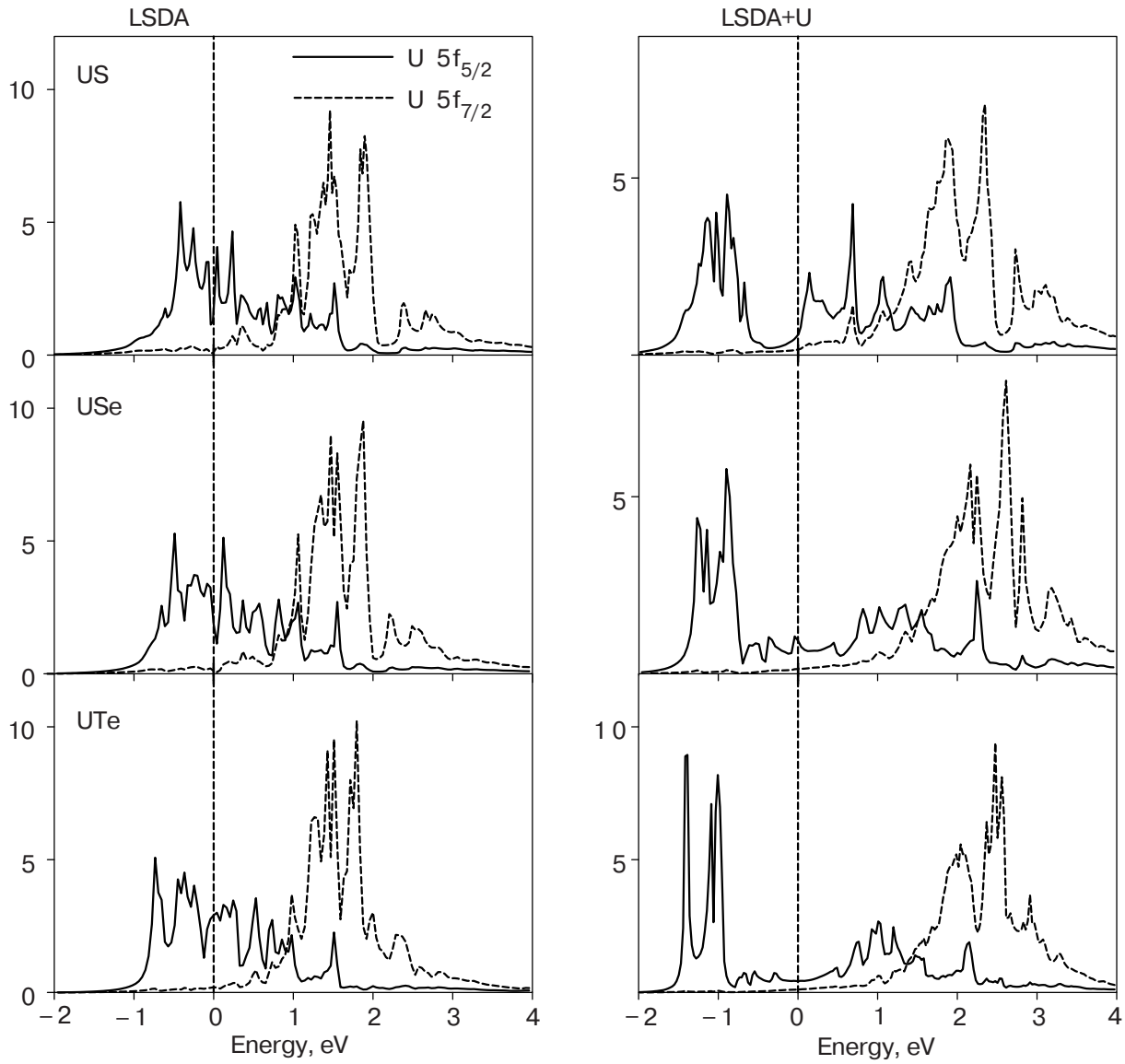

Fig. 2. The partial $5f_{5/2}$ and $5f_{7/2}$ density of states (in states/(atom·eV)) within US, USe, and UTe calculated in the LSDA and LSDA+U approximations.

with three localized $5f$ electrons in US. U $5f$ states just above the Fermi level are formed by the remaining $5f_{5/2}$ states, whereas the peak of $5f_{7/2}$ states is pushed about 1 eV upward from its LSDA position.

Figure 2 shows the calculated fully relativistic spin-polarized partial $5f$ density of states of ferromagnetic uranium monochalcogenides calculated in the LSDA and LSDA+U approximations. Because of large spin–orbit interaction of $5f$ electrons, the $j = 5/2$ and $j = 7/2$ states are fairly well separated and the occupied states are composed mostly of the $j = 5/2$ states. The $5f_{7/2}$ states are almost empty.

In magnets, the atomic spin M_s and orbital M_l magnetic moments are basic quantities and their separate determination is therefore important. Methods of their experimental determination include traditional gyromagnetic ratio measurements [73], magnetic form factor measurements using the neutron scattering [74], and magnetic x-ray scattering [75]. In addition to these, the recently developed x-ray magnetic circular dichroism combined with several sum rules [76,77] has attracted much attention as a method of site- and symmetry-selective determination of M_s and M_l. Table presents the comparison between calculated and experimental magnetic moments in uranium monochalcogenides. For comparison, we also list the results of previous band structure calculations. Our LSDA results obtained by the fully relativistic spin-polarized LMTO method are in good agreement with the ASW results of Kraft et al. [23]. The LSDA calculations for ferromagnetic uranium monochalcogenides (US, USe, and UTe) give a magnitude of the total magnetic moment M_t too small compared to the experimental

Table

The experimental and calculated spin M_s, orbital M_l, and total M_t magnetic moments at uranium site (in μ_B) of US, USe, and UTe.

Compound	Method	M_s	M_l	M_t	$-M_l/M_s$
US	LSDA	−1.53	2.14	0.60	1.41
	LSDA+U(OP)	−1.48	3.21	1.72	2.17
	LSDA+U	−1.35	3.42	2.07	2.53
	LSDA [23]	−1.6	2.5	0.9	1.6
	LSDA+OP [7]	−2.1	3.2	1.1	1.5
	OP scaled HF [78]	−1.51	3.12	1.61	2.07
	HF(TB) [27]	−1.49	3.19	1.70	2.14
	exper. [8]	−1.3	3.0	1.7	2.3
	exper. [3]	—	—	1.55	—
USe	LSDA	−1.75	2.54	0.79	1.45
	LSDA+U(OP)	−1.65	3.65	2.00	2.21
	LSDA+U	−1.96	4.61	2.65	2.35
	LSDA [23]	−1.8	2.8	1.0	1.5
	LSDA+OP [7]	−2.4	3.4	1.0	1.4
	exper. [8]	—	—	2.0	—
	exper. [3]	—	—	1.8	—
UTe	LSDA	−2.12	3.12	1.00	1.47
	LSDA+U(OP)	−1.91	4.09	2.17	2.14
	LSDA+U	−2.13	4.95	2.81	2.32
	LSDA [23]	−2.2	3.4	1.2	1.5
	LSDA+OP [7]	−2.6	3.4	0.8	1.3
	exper. [79]	−1.57	3.48	1.91	2.21
	exper. [8]	—	—	2.2	—
	exper. [3]	—	—	1.9	—

data, indicating that the calculated M_l is not large enough.

It is a well-known fact, however, that the LSDA calculations fail to produce the correct value of the orbital moment of uranium compounds [7,78,80–82]. In LSDA, the Kohn-Sham equation is described by a local potential including the spin-dependent electron density. The electric current, which describes M_l, is, however, not included. This means that although M_s is self-consistently determined in LSDA, there is no framework to simultaneously determine M_l self-consistently.

Numerous attempts have been made to better estimate M_l in solids. They can be roughly classified into two categories. One is based on the so-called current density functional theory [83–85] that is intended to extend density functional theory to include the orbital current as an extra degree of freedom, which describes M_l. Unfortunately the explicit form of the current density functional is at present unknown. The other category includes the orbital polarization (OP) [7,78, 81,82], self-interaction correction (SIC) [86], and LSDA+U [61,62] approaches, which provide a means beyond the LSDA scheme to calculate M_l.

For a better description of M_l, the OP functional form of BL_z^2 with the Racah parameter B has been deduced [7] from an atomic multiplet ground state without SOI, whose S and L are given by Hund's rules. However, the OP method does not assure us that it will give a good description when the SOI is included and thus S and L are no longer good quantum numbers. Using the LSDA+OP method Brooks [7] obtained larger magnitude of M_l and improvement in M_t. However, they have stated that the individual magnitudes of M_s and M_l are considered to be too large from the analysis of the magnetic form factor, and the ratio M_l / M_s is still far from the experimental value for all the three uranium monochalcogenides (Table).

Solovyev et al. [62] argue that the key parameter responsible for the exchange-correlation enhancement of the orbital magnetic moments in solids is the «Hubbard U» rather than the intra-atomic Hund's second rule coupling, being consistent with a more general concept of the orbital polarization. This leads to a unified rotationally invariant LSDA+U prescription for the orbital magnetism. Table presents the calculated magnetic moments in uranium monochalcogenides using a generalization of the LSDA+U method [61,62]. In this calculations we used $U = 2.0$ eV and $J = 0.5$ eV. Table presents also the LSDA+U calculated magnetic moments with $U = J = 0.5$ eV. Since in that case $U_{\text{eff}} = 0$ the effect of LSDA+U comes from non-spherical terms which are determined by F^2, F^4, and F^6 Slater integrals. Since the basic idea of such an approach is similar to the OP method [7,81], we denote the last approximation as LSDA+U(OP). The LSDA+U(OP) approximation describes the correlations between spin and orbital magnetic moment directions.

Figure 3 shows the $5f_{5/2}$ partial density of states in US calculated within the LSDA, LSDA+U(OP) and LSDA+U approximations. The LSDA+U(OP) approximation strongly affects the relative energy positions of m_j projected $5f$ density of states and substantially improves their orbital magnetic moments (Table). For example, the ratio M_l/M_s in the LSDA+U(OP) calculations is equal to −2.17 and −2.14 for US and UTe, respectively. The corresponding experimental value

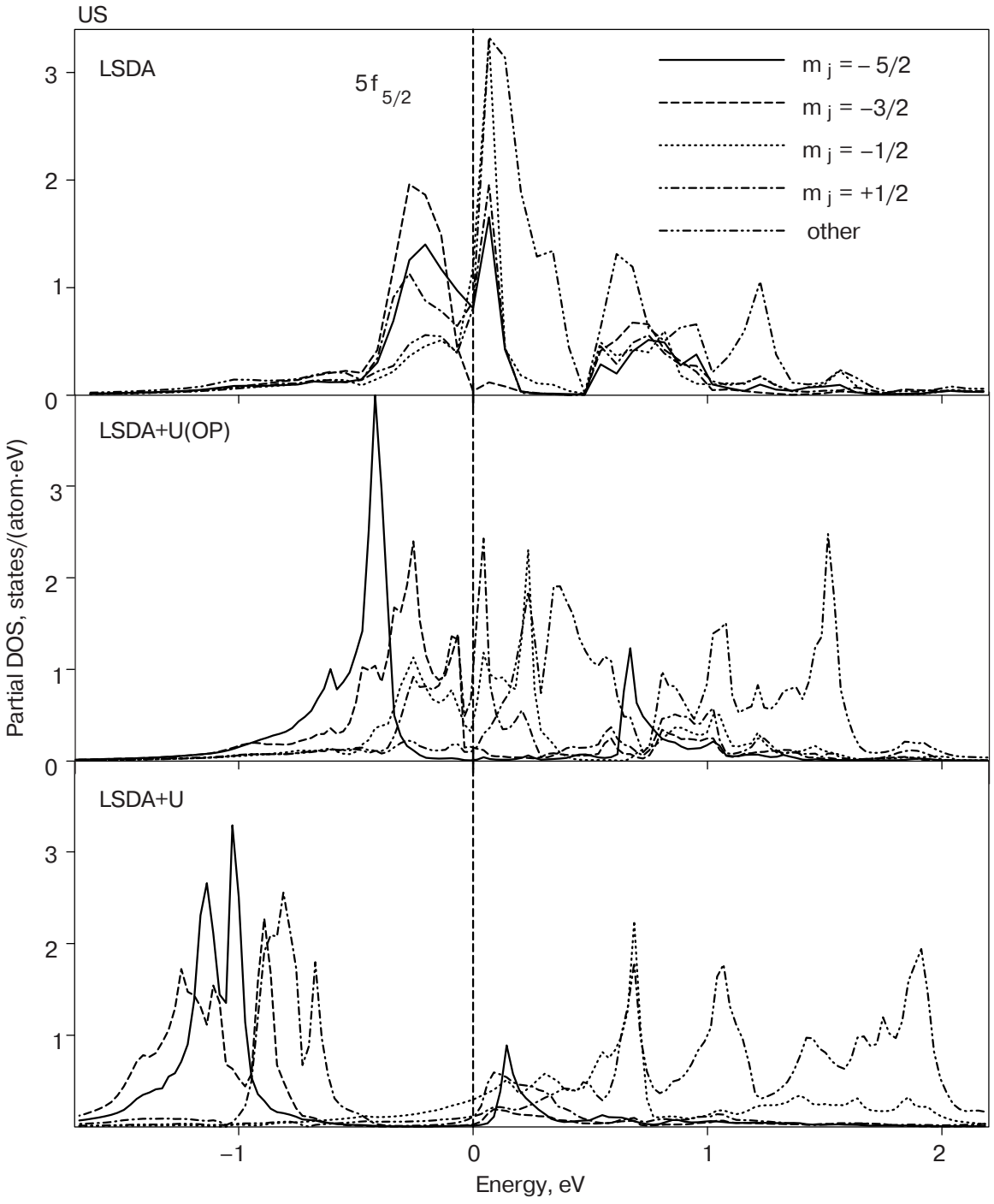

Fig. 3. The partial $5f_{5/2}$ density of states (in states/(atom·eV)) in US, USe, and UTe calculated within the LSDA, LSDA+U(OP), and LSDA+U approximations.

are −2.3 for US from the neutron measurements [8] and −2.21 for UTe from the magnetic Compton profile measurements [79].

The 5f spin M_s and orbital M_l magnetic moments in US have been also calculated in Ref. 27 on the basis of the HF approximation for an extended Hubbard model. The tight-binding model includes the intra-atomic 5f–5f multipole interaction and the SOI in the 5f state. The parameters involved in the model were determined by fitting with the energy of Bloch electrons in the paramagnetic state obtained in the LDA band structure calculation. The calculated ratio of the moments M_l/M_s of −2.14 and M_l of $-3.19\mu_B$ are in good agreement with available experimental results (Table).

We should mention that the results of the LSDA+U(OP) calculations are in close agreement

with the results obtained using the HF approximation for an extended Hubbard model [27] (Table). Both the approximations take into account the SOI and the intra-atomic $5f$–$5f$ Coulomb interaction in the Hubbard model. The small differences in magnetic moments are due to slightly different values of U_{eff}. In our calculations we used $U = J = 0.5$ eV, which gives $U_{\text{eff}} = 0$. The authors of Ref. 27 used $U = 0.76$ eV and $J = 0.5$ eV, which gives $U_{\text{eff}} = 0.26$ eV. Besides, there are some small differences in the F^2, F^4, and F^6 Slater integrals in two the calculations.

Figure 3 also shows the m_j projected $5f_{5/2}$ density of states in US calculated in the LSDA+U approximation with $U = 2.0$ eV and $J = 0.5$ eV. The corresponding partial DOSs for USe and UTe are presented in Fig. 4. The degree of localization of occupied $5f_{5/2}$ states is increasing from US to UTe. In US the $5f_{5/2}$ $f_{5/2}$ states with $m_j = -5/2$ is strongly hybridized with other occupied states, while the hybridization in USe and particularly in UTe almost vanishes. The $5f_{5/2}$ states with $m_j = -5/2$ are responsible for the narrow single peak in UTe (Fig. 4). The orbital magnetic moments calculated in the LSDA+U approximation are larger than calculated in the LSDA+U(OP) approximation, which leads to a slightly overestimated ratio M_l/M_s in comparison with the experimental data for the LSDA+U calculations (Table).

3.2. XMCD spectra

The XMCD measurements on the U $M_{4,5}$ edges of US have been presented in Ref. 29. The measured dichroic M_4 line consists of a simple nearly symmetric negative peak that has no distinct structure. Such a

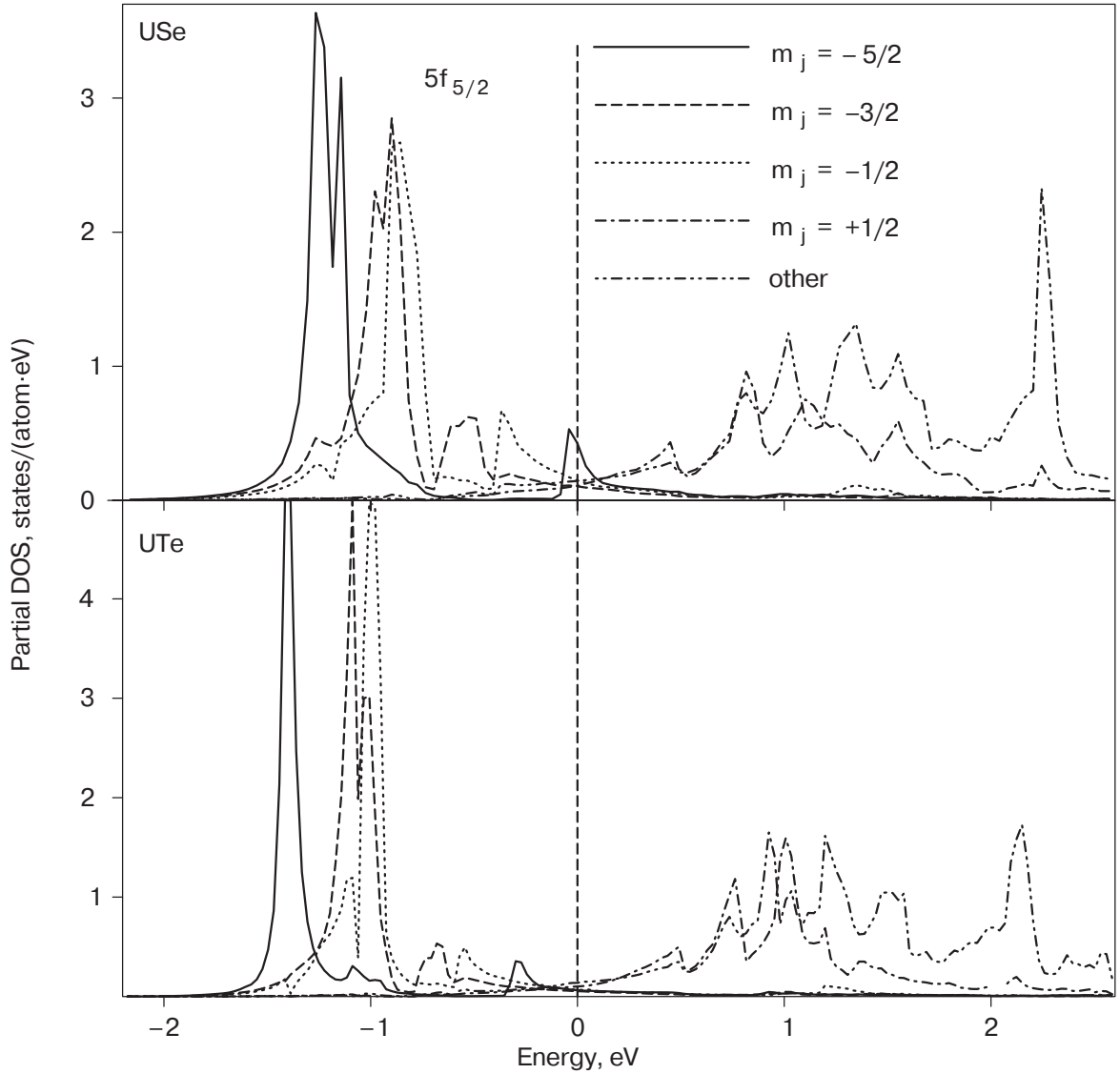

Fig. 4. The partial $5f_{5/2}$ density of states (in states/(atom·eV)) in US, USe, and UTe calculated within the LSDA+U approximation.

peak is characteristic of the M_4 edge of all uranium systems. The dichroic line at the M_5 edge has an asymmetric s shape with two peaks — a stronger negative peak and a weaker positive peak. The dichroism at the M_4 edge is more than one order of magnitude larger than at the M_5 edge.

We recall that the M_4 (M_5) edge corresponds to $3d_{3/2}(3d_{5/2}) \to 5f$ transitions. The created $3d$ core hole has electrostatic interaction with the $5f$ shell. However, in a first approximation, this interaction can be neglected since no clear multiplet structure is distinguished in the absorption spectra. This approximation is supported theoretically since the Slater integrals $F_k(3d,5f)$ and $G_k(3d,5f)$ are small compared to the $F_k(5f,5f)$ integrals and $3d$ spin-orbit interaction [29]. In neglect of the core-level splitting the measured spectra reflect the density of states above the Fermi level E_F weighted by the dipole transition probabilities. Since the XMCD technique uses circularly polarized x rays, the dichroism contains information about the character of the magnetic sublevels in the DOS.

Because of the electric dipole selection rules ($\Delta l = \pm 1$; $\Delta j = 0, \pm 1$) the major contribution to the absorption at the M_4 edge stems from the transitions $3d_{3/2} \to 5f_{5/2}$ and that at the M_5 edge originates primarily from $3d_{5/2} \to 5f_{7/2}$ transitions, with a weaker contribution from $3d_{5/2} \to 5f_{5/2}$ transitions. For the later case the corresponding $3d_{5/2} \to 5f_{5/2}$ radial matrix elements are only slightly smaller than for the $3d_{5/2} \to 5f_{7/2}$ transitions. The angular matrix elements, however, strongly suppress the $3d_{5/2} \to 5f_{5/2}$ contribution. Therefore the contribution to the XMCD spectrum at the M_5 edge from the transitions with $\Delta j = 0$ is 15 times smaller than the transitions with $\Delta j = 1$ (see Eq. 11).

Figure 5 shows the XMCD spectra of US, USe, and UTe at the uranium $M_{4,5}$ edges calculated within the LSDA and LSDA+U approximations. It is clearly seen that the LSDA calculations give inappropriate results. The major discrepancy between the LSDA calculated and experimental XMCD spectra is the size of the M_4 XMCD peak. The LSDA underestimates the integral intensity of the XMCD at M_4 edge. As the integrated XMCD signal is proportional to the orbital moment [76] this discrepancy could be related to an underestimation of the orbital moment by LSDA-based computational methods (Table). On the other hand, the LSDA+U approximation produces good agreement with the experimentally measured intensity for the M_4 XMCD spectrum. In the case of the M_5 XMCD spectrum, the LSDA strongly overestimates the value of the positive peak. The LSDA+U(OP) approximation gives good agreement in the shape and intensity of the XMCD spectrum at the M_5 edge.

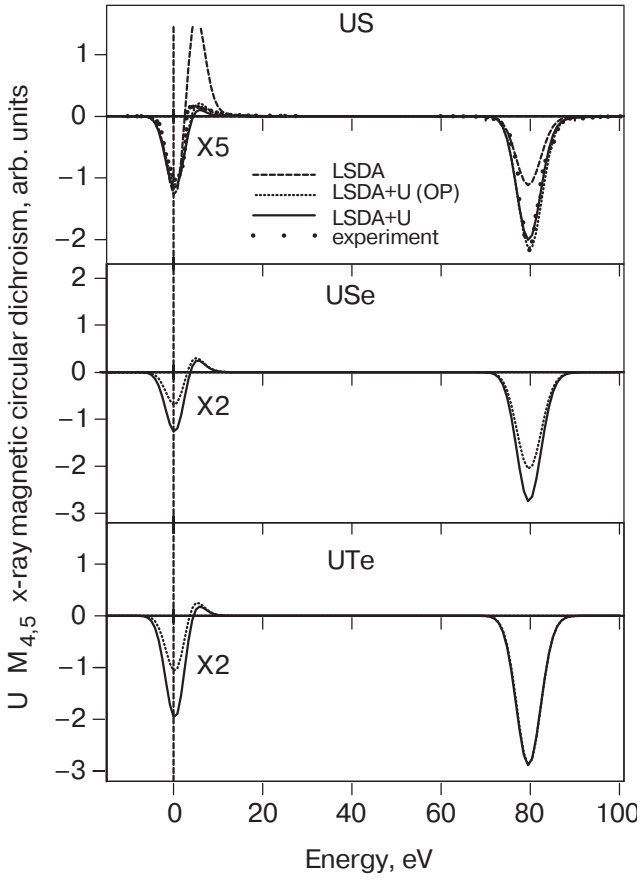

Fig. 5. The XMCD spectra of US, USe, and UTe at the uranium $M_{4,5}$ edges calculated within the LSDA (dashed lines), LSDA+U(OP) (dotted lines), and LSDA+U (solid lines) approximations. Experimental spectra of US [87] (open circles) were measured at magnetic field 2 T. The U M_4 spectra are shifted by −95 eV to include them in the figure.

The behavior of the $5f$ electrons ranges from nearly delocalized to almost localized: US is considered to be nearly itinerant [88], while UTe is considered to be quasilocalized [89]. So the failure of LSDA description of XMCD spectra in US comes as a surprise, because, if the $5f$ electrons are itinerant, one would expect the delocalized LSDA approach to be applicable. However, as the integrated XMCD signal is proportional to the orbital moment [76], this discrepancy could be related to an underestimation of the orbital moment by LSDA-based computational methods.

It is interesting to note that the LSDA+U(OP) and LSDA+U calculations give similar results for the XMCD spectrum at the M_5 edge in the case of US and became relatively more different going through USe and UTe, probably reflecting the increase of degree of

localization of the 5*f* electrons. Besides, the relative intensity of the M_5 and M_4 XMCD spectra is strongly increased going from US to UTe. Experimental measurements of the XMCD spectra in USe and UTe are highly desired.

4. Summary

We have studied by means of an initio fully-relativistic spin-polarized Dirac linear muffin-tin orbital method the electronic structure and the x-ray magnetic circular dichroism in US, USe, and UTe. We found that the degree of localization of occupied $5f_{5/2}$ states is increasing going from US to UTe. In US the 5 $f_{5/2}$ states with $m_j = -5/2$ is strongly hybridized with other occupied states, while this hybridization in USe and particularly in UTe almost vanishes. The 5 $f_{5/2}$ states with $m_j = -5/2$ form a narrow single peak in UTe.

The LSDA calculations for ferromagnetic uranium monochalcogenides (US, USe, and UTe) give the magnitude of the total magnetic moment M_t too small compared to the experimental data, indicating that the calculated M_l is not large enough. On the other hand, the LSDA+*U* method (with $U_{\text{eff}} = 0$, the so called LSDA+*U*(OP) approximation) provides good agreement with neutron and XMCD experimental data. The orbital magnetic moments calculated in the LSDA+*U* approximation are larger than calculated in the LSDA+*U*(OP) approximation, which leads to a slightly overestimated ratio M_l/M_s in comparison with the experimental data for the LSDA+*U* calculations.

The experimentally measured dichroic U M_4 line in US consists of a simple nearly symmetric negative peak that has no distinct structure. The dichroic line at the M_5 edge has an asymmetric *s* shape with two peaks — a stronger negative peak and a weaker positive peak. The major discrepancy between the LSDA calculated and experimental XMCD spectra is the size of the M_4 XMCD peak. The LSDA underestimates the integral intensity of the XMCD at the M_4 edge. As the integrated XMCD signal is proportional to the orbital moment this discrepancy could be related to an underestimation of the orbital moment by LSDA-based computational methods. The LSDA calculations also strongly overestimates the value of the positive peak of the XMCD spectrum at the M_5 edge. On the other hand, the LSDA+*U*(OP) approximation gives good agreement in the shape and intensity of the U XMCD spectra at the M_4 and M_5 edges.

Acknowledgments

This work was carried out at the Ames Laboratory, which is operated for the U.S. Department of Energy by Iowa State University under Contract No. W-7405-82. This work was supported by the Office of Basic Energy Sciences of the U.S. Department of Energy.

V.N. Antonov gratefully acknowledges the hospitality at Ames Laboratory during his stay.

1. J.-M. Fournier and R. Troch, int: *Handbook on the Physics and Chemistry of the Actinides*, A.J. Freeman and G.H. Lander (eds.), North-Holland Amsterdam (1985), V. 2, p. 29.
2. D.L. Tillwick and P. de V.du Plessis, *J. Magn. Magn. Mater.* **3**, 329 (1976).
3. G. Busch, O. Vogt, A. Delpalme, and G.H. Lander, *J. Phys.* **C12**, 1391 (1979).
4. G.H. Lander, M.S.S. Brooks, B. Lebech, P.J. Brown, O. Vogt, and K. Mattenberger, *J. Appl. Phys.* **69**, 4803 (1991).
5. M.S.S. Brooks and P.J. Kelly, *Phys. Rev. Lett.* **51**, 1708 (1983).
6. G.H. Lander, *Physica* **B186–188**, 664 (1993).
7. M.S.S. Brooks, *Physica* **B130**, 6 (1985).
8. F.A. Wedgwood, *J. Phys.* **C5**, 2427 (1972).
9. B. Reihl, *J. Less-Common Met.* **128**, 331 (1987).
10. J. Schoenes, B. Frick, and O. Vogt, *Phys. Rev.* **B30**, 6578 (1984).
11. J. Schoenes, B. Frick, and O. Vogt, *Phys. Rev.* **B30**, 6578 (1984).
12. C.Y. Huang, R.J. Laskowski, C.E. Olsen, and J.L. Smith, *J. Phys.* **C40**, 26 (1979).
13. E.F. Westrum, R.R. Walters, H.E. Flotow, and D.W. Osborne, *J. Chem. Phys.* **48**, 155 (1968).
14. P. Erdoes and J. Robinson, *The Physics of Actinide Compounds*, Plenum Press, New York, London (1983).
15. J. Neuenschwander, O. Vogt, E. Vogt, and P. Wachter, *Physica* **B144**, 66 (1986).
16. H. Bilz, G. Guentherodt, W. Kleppmann, and W. Kress, *Phys. Rev. Lett.* **43**, 1998 (1979).
17. A.L. Cornelius, J.S. Schilling, O. Vogt, K. Mattenberger, and U. Benedict, *J. Magn. Magn. Mater.* **161**, 169 (1996).
18. O.G. Sheng and B.R. Cooper, *J. Magn. Magn. Mater.* **164**, 335 (1996).
19. P. Santini, R. Lemanski, and P. Erdoes, *Adv. Phys.* **48**, 537 (1999).
20. S.V. Halilov and E.T. Kulatov, *J. Phys.: Condens. Matter* **3**, 6363 (1991).
21. T. Gasche, *Ph. D. Thesis*, Uppsala (1993).
22. B.R. Cooper, Q.G. Sheng, S.P. Lim, C. Sanchez-Castro, N. Kioussis, and J.M. Wills, *J. Magn. Magn. Mater.* **108**, 10 (1992).
23. T. Kraft, P.M. Oppeneer, V.N. Antonov, and H. Eschrig, *Phys. Rev.* **B52**, 3561 (1995).
24. J. Trygg, J.M. Wills, and M.S.S. Brooks, *Phys. Rev.* **B52**, 2496 (1995).

25. P.M. Oppeneer, V.N. Antonov, A.Y. Perlov, A.N. Yaresko, T. Kraft, and H. Eschrig, *Physica* **B230–232**, 544 (1997).
26. H. Yamagami, *J. Phys. Soc. Jpn.* **67**, 3176 (1999).
27. T. Shishidou, T. Oguchi, and T. Jo, *Phys. Rev.* **B59**, 6813 (1999).
28. T. Shishidou and T. Oguchi, *Phys. Rev.* **B62**, 11747 (2000).
29. S.P. Collins, D. Laundy, C.C. Tang, and G. van der Laan, *J. Phys.: Condens. Matter* **7**, 9325 (1995).
30. H. Ebert, *Rep. Prog. Phys.* **59**, 1665 (1996).
31. J.P. Hannon, G.T. Trammel, M. Blume, and D. Gibbs, *Phys. Rev. Lett.* **61**, 1245 (1988).
32. S.W. Lovsey and S.P. Collins, *X-Ray Scattering and Absorption in Magnetic Materials*, Oxford University Press, Oxford (1996).
33. J.B. Kortight and S.-K. Kim, *Phys. Rev.* **B62**, 12216 (2000).
34. M.I. Friezer, *IEEE Trans. Magn.* **4**, 152 (1968).
35. G.Y. Guo, *Phys. Rev.* **B55**, 11619 (1998).
36. P.N. Argyres, *Phys. Rev.* **97**, 334 (1955).
37. P.J. Durham, in: *The Electronic Structure of Complex Systems*, P. Phariseu and W.M. Temmerman (eds.), Plenum, New York (1984).
38. W.H. Kleiner, *Phys. Rev.* **142**, 318 (1966).
39. F.U. Hillebrecht, C. Roth, H.B. Rose, W.G. Park, E. Kisker, and Kirschner, *Phys. Rev.* **B55**, 2594 (1997).
40. J.G. Menchero, *Phys. Rev.* **B57**, 993 (1998).
41. G. van der Laan, *J. Magn. Magn. Mater.* **148**, 53 (1995).
42. G. van der Laan, *J. Electron. Spectrosc. Relat. Phenom.* **86**, 41 (1997).
43. G. van der Laan, *J. Phys.: Condens. Matter* **9**, L259 (1997).
44. G. van der Laan, *Phys. Rev.* **B57**, 5250 (1998).
45. J.G. Menchero, *Phys. Rev.* **B57**, 1001 (1998).
46. A. Fanelsa, R. Schellenberg, F.U. Hillebrecht, E. Kisker, J.G. Menchero, A.P. Kaduwela, C.S. Fadley, and M.A.V. Hove, *Phys. Rev.* **B54**, 17962 (1996).
47. J.G. Menchero, C.S. Fadley, G. Panaccione, F. Sirotti, G.J. Henk, and R. Feder, *Phys. Rev.* **B55**, 11476 (1997).
48. J.G. Menchero, *Phys. Rev.* **B55**, 5505 (1997).
49. R. Schellenberg, E. Kisker, A. Fanelsa, F.U. Hillebrecht, J.G. Menchero, A.P. Kaduwela, C.S. Fadley, and M.A.V. Hove, *Phys. Rev.* **B57**, 14310 (1998).
50. H. Ebert, L. Baumgarten, C.M. Schneider, and J. Kirschner, *Phys. Rev.* **B44**, 4406 (1991).
51. H. Ebert and G.Y. Guo, *J. Magn. Magn. Mater.* **148**, 178 (1995).
52. G.Y. Guo, H. Ebert, W.M. Temmerman, and P.J. Durham, *Phys. Rev.* **B50**, 3861 (1994).
53. E. Tamura, G.D. Waddill, J.G. Tobin, and P.A. Sterne, *Phys. Rev. Lett.* **73**, 1533 (1994).
54. V.N. Antonov, A.I. Bagljuk, A.Y. Perlov, V.V. Nemoshkalenko, Vl.N. Antonov, O.K. Andersen, and O. Jepsen, *Fiz. Nizk. Temp.* **19**, 689 (1993) [*Low Temp. Phys.* **19**, 494 (1993)].
55. V.V. Nemoshkalenko, V.N. Antonov, V.N. Antonov, W. John, H. Wonn, and P. Ziesche, *Phys. Status Solidi* **B111**, 11 (1982).
56. V.I. Anisimov, J. Zaanen, and O.K. Andersen, *Phys. Rev.* **B44**, 943 (1991).
57. P.W. Anderson, *Phys. Rev.* **124**, 41 (1961).
58. J. Hubbard, *Proc. R. Soc. London, Ser. A* **276**, 238 (1963).
59. J. Hubbard, *Proc. R. Soc. London, Ser. A* **277**, 237 (1964).
60. V.I. Anisimov, I.V. Solovyev, M.A. Korotin, M.T. Czyzyk, and G.A. Sawatsky, *Phys. Rev.* **B48**, 16929 (1993).
61. A.N. Yaresko, V.N. Antonov, and P. Fulde, *Phys. Rev.* **B67**, 155103 (2003).
62. I.V. Solovyev, A.I. Liechtenstein, and K. Terakura, *Phys. Rev. Lett.* **80**, 5758 (1998).
63. H. Harima, *J. Magn. Magn. Mater.* **226–230**, 83 (2001).
64. C. Herring, in: *Magnetism*, G.T. Rado and H. Suhl (eds.), Academic, New York (1966), V. IV.
65. V.I. Anisimov and O. Gunnarsson, *Phys. Rev.* **B43**, 7570 (1991).
66. P.H. Dederichs, S. Blügel, R. Zeller, and H. Akai, *Phys. Rev. Lett.* **53**, 2512 (1984).
67. I.V. Solovyev, P.H. Dederichs, and V.I. Anisimov, *Phys. Rev.* **B50**, 16861 (1994).
68. W.E. Pickett, S.C. Erwin, and E.C. Ethridge, *Phys. Rev.* **B58**, 1201 (1998).
69. V.N. Antonov, B.N. Harmon, and A.N. Yaresko, *Phys. Rev.* **B63**, 205112, (2001).
70. V.N. Antonov, B.N. Harmon, and A.N. Yaresko, *Phys. Rev.* **B66**, 165208 (2002).
71. U. von Barth and L. Hedin, *J. Phys.* **C5**, 1629 (1972).
72. P.E. Blöchl, O. Jepsen, and O.K. Andersen, *Phys. Rev.* **B49**, 16 (1994).
73. G.G. Scott, *J. Phys. Soc. Jpn.* **17**, 372 (1962).
74. W. Marshall and S.W. Lovsey, *Theory of Thermal Neutron Scattering*, Oxford University Press, Oxford (1971).
75. M. Blume, *J. Appl. Phys.* **57**, 3615 (1985).
76. B.T. Thole, P. Carra, F. Sette, and G. van der Laan, *Phys. Rev. Lett.* **68**, 1943 (1992).
77. P. Carra, B.T. Thole, M. Altarelli, and X. Wang, *Phys. Rev. Lett.* **70**, 694 (1993).
78. L. Severin, M.S.S. Brooks, and B. Johansson, *Phys. Rev. Lett.* **71**, 3214 (1993).
79. H. Sakurai, H. Hashimoto, A. Ochiai, T. Suzuki, M. Ito, and F. Itoh, *J. Phys.: Condens. Matter* **7**, L599 (1995).
80. M.S.S. Brooks and B. Johansson, in: *Handbook of Magnetic Materials*, K.H.J. Buschow (ed.), Amsterdam, North-Holland, (1993), V. 7, p. 139
81. O. Eriksson, M.S.S. Brooks, and B. Johansson, *Phys. Rev.* **B41**, 7311 (1990).
82. A. Mavromaras, L. Sandratskii, and J. K«ubler, *Solid State Commun.* **106**, 115 (1998).
83. G. Vignale and M. Rasolt, *Phys. Rev. Lett.* **59**, 2360 (1987).

84. P. Skudlarski and G. Vigmale, *Phys. Rev*. **B48**, 8547 (1993).
85. M. Higuchi and A. Haegawa, *J. Phys. Soc. Jpn.* **66**, 149 (1997).
86. S.V. Beiden, W.M. Temmerman, Z. Szotek, and G.A. Gehring, *Phys. Rev. Lett.* **79**, 4970 (1997).
87. M. Kucera, J. Kunes, A. Kolomiets, M. Divis, A.V. Andreev, V. Sechovsky, J.P. Kappler, and A. Rogalev, *Phys. Rev*. **B66**, 144405 (2002).
88. M.S.S. Brooks, T. Gasche, and B. Johansson, *J. Phys. Chem. Solids* **56**, 1491 (1995).
89. B. Reihl, N. Martensson, and O. Vogt, *J. Appl. Phys.* **53**, 2008 (1982).